POLARIZATION EFFECTS IN RESONANT 4-WAVE-MIXING PROCESSES

Aben, I.; Ubachs, W.M.G.; van der Zwan, G.; Hogervorst, W.

published in
Molecular Physics
1992

DOI (link to publisher)
10.1080/00268979200101551

document version
Publisher's PDF, also known as Version of record

MOLECULAR PHYSICS, 1992, VOL. 76, NO. 3, 591–608

Polarization effects in resonant four-wave-mixing processes

By ILSE ABEN, WIM UBACHS, GERT VAN DER ZWAN and WIM HOGERVORST

Laser Centre, Free University Amsterdam, De Boelelaan 1081, 1081 HV Amsterdam, The Netherlands

(*Received 17 December 1991; accepted 14 January 1992*)

Theoretical expressions for rotational linestrengths in four-wave-mixing (FWM) processes are derived and compared with observed linestrengths in multiple resonant coherent anti-Stokes–Raman scattering (CARS) processes in I_2. General expressions for coherent four-photon transitions are deduced that are applicable for numerical evaluation of rotational linestrengths in a wide variety of different FWM processes. For several FWM resonance schemes, such as parametric and non-parametric excited state CARS, closed-form algebraic expressions are deduced for the J-dependent linestrengths in a Hunds' case (c) coupling case. In the experimental part of the study intensity ratios between line doublets in the FWM spectra probing the same ground state populations are measured for arbitrary (but linear) polarization orientation of two incoming waves ω_1 and ω_2. For both the parametric and the non-parametric resonant FWM processes, the experimental intensity ratios are compared with theory and satisfactory agreement is found.

1. Introduction

Coherent four-wave-mixing (FWM) processes are widely used for non-intrusive, remote probing of hostile environments. The sensitivity of FWM processes is enhanced when electronic resonances are accessible. Resonance-enhanced FWM is employed to study species in flames or combustion engines, either by using degenerate FWM (DFWM) or non-degenerate FWM, e.g. coherent anti-Stokes Raman scattering (CARS). DFWM has been used to detect OH [1, 2] and NH [2] in flames. Resonance enhancement through bound states in CARS has been shown for I_2 [3, 4], OH [5], C_2 [6], and NO_2 [7, 8]. Apart from the effect of bound states, also resonance-enhancement on dissociative continuum states at the one-photon level ($^1\Pi_{1u}$ and above $B^3\Pi^+_{u0}$) and the two-photon (0^+_g) level was investigated in I_2 [4, 9].

Derivation of rotational linestrengths in FWM processes is required to evaluate DFWM and resonance CARS data in terms of density and temperature of the media. The calculation of four-photon coherent linestrengths involves the elaborate mathematical task of summing over all degenerate M_J states in a four-photon sequence. Several years ago Mainos *et al.* [10] derived a general formula for the rotational line strength in multiphoton transitions between two Hund's case (a) states in diatomic molecules. In the case of third-harmonic generation in CO different groups [11, 12] have calculated and measured line intensities for specific four-wave-mixing schemes. More recently, Attal-Trétout *et al.* [13] presented rotational linestrength calculations for diatomics for various resonant CARS and Hund's coupling schemes, thus closed-form expressions for rotational linestrengths for a number of different FWM processes are available. These studies were, however, restricted to a wave-geometry, with

0026–8976/92 $3.00

$\boldsymbol{k}$ vectors of incoming and outgoing waves parallel, and in most cases polarizations of the waves linear and parallel.

Iodine vapour is a favourable medium for an experimental study of resonance enhancement in FWM processes. Electronic transitions in the spectroscopically well characterized $B^3\Pi_{u0}^+ - X^1\Sigma_g^+$ band system [14] are within the visible wavelength region. The present work is an extension of a previous study in which several resonant FWM processes were identified on the basis of line positions [4]. Now, line intensities are investigated as a function of polarization for two of these processes, namely the parametric and non-parametric excited-state CARS, both experimentally and theoretically. In the experimental part a $\omega = 2\omega_1 - \omega_2$ type FWM process was investigated in a configuration where both incoming beams were linearly polarized, and the relative polarization orientation of the beams was varied from parallel to crossed. For the two extreme cases, parallel and crossed polarization, closed-form theoretical expressions for the rotational line strengths are derived.

The quantitative interpretation of linestrengths in resonance-enhanced CARS spectra is not simple, because they do not only depend on the evaluation of four-photon transition moments but also on detunings from resonance represented by denominators in the expression for the non-linear susceptibility and on population densities. We, therefore, derived intensity ratios of lines appearing in the spectra as doublets. The factors containing the detunings cancel when the ratio of line intensities in specific doublets is taken. The experimental ratios can be compared with the closed-form expressions which are derived and tabulated. For the two particular CARS processes experimentally investigated, we find satisfactory agreement between theory and observation for each arbitrary direction of the polarization vectors.

2. Theoretical framework

2.1. *General*

In a FWM process a fourth wave at a frequency $\omega = \pm\omega_1 \pm \omega_2 \pm \omega_3$ is created out of three incoming waves with frequencies ω_1, ω_2 and ω_3. The intensity of the generated wave is proportional to the absolute square of the induced non-linear polarization [15]:

$$I(\omega) \propto |\boldsymbol{P}_{NL}(\omega)|^2 = |\overline{\overline{\chi}}^{(3)}(\omega) : \boldsymbol{E}(\omega_1)\boldsymbol{E}(\omega_2)\boldsymbol{E}(\omega_3)|^2, \tag{1}$$

in which $\overline{\overline{\chi}}^{(3)}(\omega)$ is the third-order non-linear susceptibility tensor of rank four. The electric field of the incoming wave with frequency ω_i is denoted by $\boldsymbol{E}(\omega_i)$. The different cartesian components of the induced nonlinear polarization can be written as

$$P_\rho^{NL}(\omega) = \sum_{\sigma\tau\nu} \chi^{(3)}_{\rho\sigma\tau\nu}(\omega)\boldsymbol{E}_\sigma(\omega_1)E_\tau(\omega_2)E_\nu(\omega_3). \tag{2}$$

In the following we restrict ourselves to the case of FWM processes with two different incoming beams, one with a frequency ω_1 and one with a frequency ω_2. Both beams have linear polarization. A wave at frequency $\omega = 2\omega_1 - \omega_2$ is generated. A coordinate system is chosen such that the y-axis coincides with the propagation vectors $\boldsymbol{k}$ of all waves, and the laboratory fixed z-axis is parallel to $\boldsymbol{E}(\omega_1)$. An arbitrary angle α between the polarizations of the incoming beams is assumed. The electric field components of the ω_1- and ω_2-beam may thus be written as

$$\begin{aligned} \boldsymbol{E}(\omega_1) &= E^1(\omega_1)\boldsymbol{e}_z, \\ \boldsymbol{E}(\omega_2) &= E^2(\omega_2)[(\cos\alpha\,\boldsymbol{e}_z + \sin\alpha\,\boldsymbol{e}_x), \end{aligned} \tag{3}$$

where e_z and e_x are unit vectors along the z- and x-axis, respectively.

The different components of the induced nonlinear polarization can be expressed as

$$\begin{aligned} P_x &= E^1 E^1 E^{2*}(\chi^{(3)}_{xzzx}\sin\alpha + \chi^{(3)}_{xzzz}\cos\alpha), \\ P_y &= E^1 E^1 E^{2*}(\chi^{(3)}_{yzzx}\sin\alpha + \chi^{(3)}_{yzzz}\cos\alpha), \\ P_z &= E^1 E^1 E^{2*}(\chi^{(3)}_{zzzx}\sin\alpha + \chi^{(3)}_{zzzz}\cos\alpha). \end{aligned} \tag{4}$$

For an isotropic system it will be shown that the elements $\chi^{(3)}_{xzzz}$, $\chi^{(3)}_{yzzx}$, $\chi^{(3)}_{yzzz}$ and $\chi^{(3)}_{zzzx}$ are zero, so, for an isotropic medium the intensity of the generated wave is proportional to

$$I \propto |\chi^{(3)}_{xzzx}|^2 \sin^2\alpha + |\chi^{(3)}_{zzzz}|^2 \cos^2\alpha. \tag{5}$$

Of the 81 elements of the fourth-rank tensor $\chi^{(3)}$ only two, $\chi^{(3)}_{xzzx}$ and $\chi^{(3)}_{zzzz}$, bear relevance for the present analysis. It is important to note that the non-linear susceptibility tensor $\chi^{(3)}$ is a property of the medium and does not depend on the applied fields.

In the most general case of a FWM process with a wave generated at frequency $\omega = \pm\omega_1 \pm \omega_2 \pm \omega_3$, a 48 term expression for $\chi^{(3)}(\omega)$ results [16]. When the frequency of the generated wave is $\omega_3 = 2\omega_1 - \omega_2$, like in CARS, $\chi^{(3)}(\omega_3)$ contains 24 terms. In general these terms have the following form (see [4])

$$\chi^{(3)}_{\rho\sigma\tau\nu}(\omega_3) = N \sum_{0,a,b,c} \rho^{(0)}_{00} \frac{\langle 0|\mu_\sigma|a\rangle\langle a|\mu_\tau|b\rangle\langle b|\mu_\nu|c\rangle\langle c|\mu_\rho|0\rangle}{(\omega_{a0} - \omega_1 - i\Gamma_{a0})(\omega_{b0} - \omega_1 + \omega_2 - i\Gamma_{b0})(\omega_{c0} - \omega_3 - i\Gamma_{c0})}. \tag{6}$$

Here $|0\rangle$, $|a\rangle$, $|b\rangle$ and $|c\rangle$ are rovibronic molecular states and μ_σ is the component of the transition dipole moment vector in the laboratory frame along the Cartesian σ axis. $\rho^{(0)}_{00}$ represents the relative population distribution over initial quantum states $|J\Omega M\rangle$ of the system. It also includes a nuclear spin statistics factor, which is $\frac{7}{12}$ for odd J states and $\frac{5}{12}$ for even J states. The summations over ground states $|0\rangle$ and excited states $|a\rangle$, $|b\rangle$ and $|c\rangle$ refer to all possible resonances in the spectrum. Only contributions from FWM processes probing a population density $N\rho^{(0)}_{00}$ in the ground state $|0\rangle$ are considered. In multiple-resonant CARS the intensity at a particular resonance in the FWM spectrum is dominated by one or just a few terms in $\chi^{(3)}$. Moreover, at a specific wavelength combination, only some definite states $|0\rangle$, $|a\rangle$, $|b\rangle$ and $|c\rangle$ are involved [4]. At resonance all summations over non-degenerate states are, therefore, dropped. For degenerate states, such as the M components of a rotational state J, the summation is maintained. In case one of the states $|a\rangle$, $|b\rangle$ and $|c\rangle$ represents a continuum, contributions of all possible J-states are considered and all possible routes through the continuum in terms of four-state cycles are accounted for.

In the numerator of a specific $\chi^{(3)}$ term, assuming four discrete levels $|0\rangle$, $|a\rangle$, $|b\rangle$ and $|c\rangle$, a sum of products of four transition dipole matrix elements occurs:

$$\chi^{(3)}_{\rho\sigma\tau\nu} \propto \sum_{M_0,M_a,M_b,M_c} \langle 0|\mu_\sigma|a\rangle\langle a|\mu_\tau|b\rangle\langle b|\mu_\nu|c\rangle\langle c|\mu_\rho|0\rangle. \tag{7}$$

For a calculation of rotational line strengths we focus on this product of the transition moments. At this point the product of three 'resonance factors' in the denominator of $\chi^{(3)}$ and the factor $N\rho^{(0)}_{00}$ are not considered.

In the Born–Oppenheimer approximation the wavefunction of a state $|a\rangle$ may be represented by a separate electronic, vibrational and rotational part:

$$|\mathrm{a}\rangle = |\phi_a^{\mathrm{electr.}}\rangle|\Phi_{v_a}^{\mathrm{vib.}}\rangle|\mathrm{J}_a\Omega_a\mathrm{M}_a\rangle. \tag{8}$$

Here J is the total angular momentum and Ω is its projection onto the internuclear axis. In the case of a diatomic Ω is also the projection of the electronic angular momentum onto the internuclear axis [17]. M is the projection of J on a space fixed axis.

The dot product of the transition dipole vector and the vector representing the polarization orientation of the electric field may be written in spherical tensor notation [17]:

$$\mu_p^{(L)} = \boldsymbol{\mu}^{(\mathrm{L})} \cdot \boldsymbol{e}^{p(\mathrm{L})} = \sum_{m=0,\pm 1} (-1)^m \boldsymbol{\mu}_m^{(L)} e_{-m}^{p(L)}, \tag{9}$$

where e^p_{-m} denotes the component of the polarization of the corresponding field on the spherical m axis. The cartesian components of the transition dipole moment are related to the spherical components as [17]:

$$\begin{aligned} \mu_z &= \mu_0, \\ \mu_x &= \frac{1}{\sqrt{2}}(\mu_{-1} - \mu_1), \\ \mu_y &= \frac{i}{\sqrt{2}}(\mu_{-1} + \mu_1). \end{aligned} \tag{10}$$

To evaluate the matrix elements, the dipole moment operator $\boldsymbol{\mu}^{(\mathrm{L})}$ in the laboratory or space-fixed frame must be transformed to the molecular frame $\boldsymbol{\mu}^{(\mathrm{M})}$:

$$\mu_m^{(\mathrm{L})} = \sum_{m'} D_{mm'}^{(1)*}(\alpha\beta\gamma)\mu_{m'}^{(\mathrm{M})}. \tag{11}$$

Here $D_{mm'}^{(1)}$ are the Wigner rotation matrix elements, and α, β and γ are the Euler angles. (This α should not be confused with the relative polarization orientation α introduced in (3)). Using (9) this leads to

$$\mu_p^{(L)} = \boldsymbol{\mu}^{(\mathrm{L})} \cdot \boldsymbol{e}^{p(\mathrm{L})} = \sum_{m=0,\pm 1} \sum_{m'=0,\pm 1} (-1)^m D_{mm'}^{(1)*}(\alpha\beta\gamma)\mu_{m'}^{(\mathrm{M})} e_{-m}^{p(\mathrm{L})}. \tag{12}$$

The rotational wavefunctions are [17]

$$|\mathrm{J}\Omega\mathrm{M}\rangle = (-1)^{M-\Omega}\left(\frac{2J+1}{8\pi^2}\right)^{1/2} D^J_{-M\ -\Omega}(\alpha\beta\gamma). \tag{13}$$

Using this expression the individual matrix elements for dipole allowed transitions between arbitrary states $|\mathrm{a}\rangle$ and $|\mathrm{b}\rangle$ may be expressed as

$$\begin{aligned} \langle \mathrm{a}|\mu_p^{(\mathrm{L})}|\mathrm{b}\rangle &= \langle \mathrm{a}|\boldsymbol{\mu}^{(\mathrm{L})} \cdot \boldsymbol{e}^{p(\mathrm{L})}|\mathrm{b}\rangle = \langle \mathrm{a}| \sum_{m=0,\pm 1} (-1)^m \mu_m^{(\mathrm{L})} e_{-m}^{p(L)}|\mathrm{b}\rangle \\ &= \sum_{mm'} (-1)^m e_{-m}^{p(L)} \langle \phi_a^{\mathrm{electr.}}|\mu_{m'}^{(\mathrm{M})}|\phi_b^{\mathrm{electr.}}\rangle \langle \Phi_{v_a}^{\mathrm{vib.}}|\Phi_{v_b}^{\mathrm{vib.}}\rangle \\ &\quad \times \langle \mathrm{J}_a\Omega_a\mathrm{M}_a|D_{mm'}^{(1)*}(\alpha\beta\gamma)|\mathrm{J}_b\Omega_b\mathrm{M}_b\rangle. \end{aligned} \tag{14}$$

In this equation the vibrational overlap function

$$F_{ab} = \langle \Phi_{v_a}^{\mathrm{vib.}}|\Phi_{v_b}^{\mathrm{vib.}}\rangle \tag{15}$$

may be separated off; $|F_{ab}|^2$ represents the Franck–Condon factor of the transition. The electronic transition matrix element is defined as

$$\mu_{ab}^{m'(M)} = \langle \phi_a^{\mathrm{electr.}}|\mu_{m'}^{(\mathrm{M})}|\phi_b^{\mathrm{electr.}}\rangle. \tag{16}$$

The rotational part of a single transition moment can be evaluated using the closure relation:

$$\langle \mathrm{J}_a \Omega_a \mathrm{M}_a | D^{(1)*}_{mm'}(\alpha\beta\gamma) | \mathrm{J}_b \Omega_b \mathrm{M}_b \rangle$$
$$= \left(\frac{2J_b + 1}{2J_a + 1}\right)^{1/2} (-1)^{m+m'} \delta_{M_a - m - M_b, 0} \delta_{\Omega_a - m' - \Omega_b, 0} \langle J_b, -\mathrm{M}_b, 1, -\mathrm{m} | \mathrm{J}_a, -\mathrm{M}_b - \mathrm{m} \rangle$$
$$\times \langle \mathrm{J}_b, -\Omega_b, 1, -\mathrm{m}' | \mathrm{J}_a, -\Omega_b - \mathrm{m}' \rangle. \tag{17}$$

In (17) the last two factors written in brackets denote Clebsch–Gordan coefficients using the notation of Zare [17]. Using expressions (14)–(17) the term involving a product of four transition moments yields

$$\chi^{(3)}_{\rho\sigma\tau\nu} \propto \sum_{jklm} \sum_{j'k'l'm'} \sum_{M_0, M_a, M_b, M_c} e^{\sigma}_{-k} e^{\tau}_{-l} e^{\nu}_{-m} e^{\rho}_{-j} \mu^{k'(M)}_{0a} \mu^{l'(M)}_{ab} \mu^{m'(M)}_{bc} \mu^{j'(M)}_{c0} (-1)^{k'+l'+m'+j'} F_{0a} F_{ab} F_{bc} F_{c0}$$
$$\times \delta_{M_0 \; k \; M_a, 0} \delta_{\Omega_0 \; k' \; \Omega_a, 0} \langle \mathrm{J}_a, k - \mathrm{M}_0, 1, -k | \mathrm{J}_0, -\mathrm{M}_0 \rangle \langle \mathrm{J}_a, k' - \Omega_0, 1, -k' | \mathrm{J}_0, -\Omega_0 \rangle$$
$$\times \delta_{M_a - l - M_b, 0} \delta_{\Omega_a - l' - \Omega_b, 0} \langle \mathrm{J}_b, l - \mathrm{M}_a, 1, -l | \mathrm{J}_a, -\mathrm{M}_a \rangle \langle \mathrm{J}_b, l' - \Omega_a, 1, -l' | \mathrm{J}_a, -\Omega_a \rangle$$
$$\times \delta_{M_b - m - M_c, 0} \delta_{\Omega_b - m' - \Omega_c, 0} \langle \mathrm{J}_c, m - \mathrm{M}_b, 1, -m | \mathrm{J}_b, -\mathrm{M}_b \rangle \langle \mathrm{J}_c, m' - \Omega_b, 1, -m' | \mathrm{J}_b, -\Omega_b \rangle$$
$$\times \delta_{M_c - j - M_0, 0} \delta_{\Omega_c - j' - \Omega_0, 0} \langle \mathrm{J}_0, j - \mathrm{M}_c, 1, -j | \mathrm{J}_c, -\mathrm{M}_c \rangle \langle \mathrm{J}_0, j' - \Omega_c, -j' | \mathrm{J}_c, -\Omega_c \rangle. \tag{18}$$

The summation over all degenerate M-states is maintained. The characteristic of rotational linestrengths in a coherent multiphoton process such as FWM, is that summations over all degenerate states M have to be performed simultaneously. This is in contrast to the case of non-coherent multi-step processes where the linestrengths of consecutive single one-photon transitions are multiplied.

Evaluating all δ-functions relation (18) reduces to

$$\chi^{(3)}_{\rho\sigma\tau\nu} \propto \sum_{jklm} e^{\sigma}_{-k} e^{\tau}_{-l} e^{\nu}_{-m} e^{\rho}_{-j} \mu^{\Omega_0 - \Omega_a}_{0a} \mu^{\Omega_a - \Omega_b}_{ab} \mu^{\Omega_b - \Omega_c}_{bc} \mu^{\Omega_c - \Omega_0}_{c0} F_{0a} F_{ab} F_{bc} F_{c0} S^{0abc}_{jklm}. \tag{19}$$

Here S^{0abc}_{jklm} is the CARS rotational line strength factor

$$S^{0abc}_{jklm} = \langle \mathrm{J}_a, -\Omega_a, 1, \Omega_a - \Omega_0 | \mathrm{J}_0, -\Omega_0 \rangle \langle \mathrm{J}_b, -\Omega_b, 1, \Omega_b - \Omega_a | \mathrm{J}_a, -\Omega_a \rangle$$
$$\times \langle \mathrm{J}_c, -\Omega_c, 1, \Omega_c - \Omega_b | \mathrm{J}_b, -\Omega_b \rangle \langle \mathrm{J}_0, -\Omega_0, 1, \Omega_0 - \Omega_c | \mathrm{J}_c, -\Omega_c \rangle$$
$$\times \sum_{M_0} \delta_{k+l+m+j, 0} \langle \mathrm{J}_a, k - \mathrm{M}_0, 1, -k | \mathrm{J}_0, -\mathrm{M}_0 \rangle \langle \mathrm{J}_b, l + k - \mathrm{M}_0, 1, -l | \mathrm{J}_a, k - \mathrm{M}_0 \rangle$$
$$\times \langle \mathrm{J}_c, m + l + k - \mathrm{M}_0, 1, -m | \mathrm{J}_b, k + 1 - \mathrm{M}_0 \rangle$$
$$\times \langle \mathrm{J}_0, -\mathrm{M}_0, 1, -j | \mathrm{J}_c, k + l + m - \mathrm{M}_0 \rangle. \tag{20}$$

S^{0abc}_{jklm} contains a product of two parts. One part only depends on the projection of the electronic angula momentum on the internuclear axis (Ω), and on the specific J routes. The other part is determined by the polarizations, J routes and the sum over all M_0 components.

The summation over M_0 components in (20) refers to all possible orientations in space of the ensemble of molecules in the gas phase, which should be considered in an isotropic medium. The linestrength factor S^{0abc}_{jklm} is defined in a spherical basis. It is easily seen from (20) and the transformation from a cartesian to a spherical basis as given in (10), that the Cartesian elements $\chi^{(3)}_{xzzz}$, $\chi^{(3)}_{yzzx}$, $\chi^{(3)}_{yzzz}$ and $\chi^{(3)}_{zzzx}$ are equal to zero as assumed in the derivation of (5).

Table 1. Rotational line strength factors S for a Hund's case (c), where $\Omega_0 = \Omega_a = \Omega_b = \Omega_c = 0$.

	Parallel polarization[a]	Crossed polarization
$[J, J-1, J-2, J-1]$	$\frac{2J(J-1)}{15(2J-1)}$	$\frac{J(J-1)}{15(2J-1)}$
$[J, J-1, J, J-1]$	$\frac{J(4J^2+1)}{15(2J+1)(2J-1)}$	$\frac{-J(J-1)(6J+1)}{30(2J-1)(2J+1)}$
$[J, J-1, J, J+1]$	$\frac{2J(J+1)}{15(2J+1)}$	$\frac{-J(J+1)}{10(2J+1)}$
$[J, J+1, J, J-1]$	$\frac{2J(J+1)}{15(2J+1)}$	$\frac{-J(J+1)}{10(2J+1)}$
$[J, J+1, J+2, J+1]$	$\frac{2(J+1)(J+2)}{15(2J+3)}$	$\frac{(J+1)(J+2)}{15(2J+3)}$
$[J, J+1, J, J+1]$	$\frac{(J+1)(4J^2+8J+5)}{15(2J+1)(2J+3)}$	$\frac{-(J+1)(J+2)(6J+5)}{30(2J+1)(2J+3)}$

[a] These expressions are identical to the relations given by Attal *et al.* [3]. In all tables $J = J_0$.

In general the polarization of the generated wave can be deduced from (2) when the polarizations of the incoming waves are substituted. The δ function in (20) shows that only a few $\chi^{(3)}$ elements are different from zero. Furthermore, symmetry relations for the $\chi^{(3)}$ elements can be used, which can all be deduced from (19). For the special case of linearly and parallel polarized light, k, l, and m are all equal to zero. The δ-function in (20) yields $j = 0$. This implies that the generated wave is also linearly polarized parallel to the incoming waves. When the ω_1 and ω_2 beams are linearly polarized but with crossed polarization, the generated wave is also crossed polarized to the ω_1 beam.

The expression in (20) is applicable to all cases of FWM, and the summation over all M_0s can always be performed numerically to evaluate the rotational line strengths. For some particular cases which are relevant for our experimental study, namely those for which Ω_0, Ω_a and Ω_c are zero, we derived closed-form expressions using the algebraic evaluation computer code of Mathematica™. Resulting expressions are tabulated in table I assuming the total angular momentum of all four states involved in the FWM cycle to be zero: $\Omega_0 = \Omega_a = \Omega_b = \Omega_c = 0$. In table 2 the values for a FWM sequence with $\Omega_0 = \Omega_a = \Omega_c = 0$ and $\Omega_b = 1$ are listed. In both tables the expressions are given for linearly polarized light, for the case where all beams have parallel polarization as well as for the situation where the polarization vectors of beams with ω_1 and ω_2 are perpendicular.

In tables 1 and 2 the expressions are given for any allowed combination of J state resonances in the FWM process. The selection rules for these J combinations are determined by the Clebsch–Gordan coefficients in (17). These are $\Delta J = \pm 1$ for $\Omega = 0 \leftrightarrow \Omega = 0$, and $\Delta J = 0, \pm 1$ in all other cases, for the one-photon resonances. This gives, for the case of all Ωs being zero, six allowed J combinations. For the case of $\Omega_0 = \Omega_a = \Omega_c = 0$ and $\Omega_b = 1$, there are eight allowed combinations/routes. We denote these different routes by their unique J combination $[J_0, J_a, J_b, J_c]$. The closed-form expressions in tables 1 and 2 are applicable to any FWM or coherent

Table 2. Rotational line strength factors S for a Hund's case (c), where $\Omega_0 = \Omega_a = \Omega_c = 0$ and $\Omega_b = 1$.

	Parallel polarization	Crossed polarization
$[J, J-1, J, J+1]$	$\frac{J(J+1)}{15(2J+1)}$	$\frac{-J(J+1)}{20(2J+1)}$
$[J, J-1, J, J-1]$	$\frac{-(J+1)(4J^2+1)}{30(2J-1)(2J+1)}$	$\frac{(J-1)(J+1)(6J+1)}{60(2J-1)(2J+1)}$
$[J, J-1, J-1, J-1]$	$\frac{-(J+1)}{30}$	$\frac{-(J+1)}{60}$
$[J, J-1, J-2, J-1]$	$\frac{-J(J-2)}{15(2J-1)}$	$\frac{-J(J-2)}{30(2J-1)}$
$[J, J+1, J, J-1]$	$\frac{J(J+1)}{15(2J+1)}$	$\frac{-J(J+1)}{20(2J+1)}$
$[J, J+1, J, J+1]$	$\frac{-J(4J^2+8J+5)}{30(2J+1)(2J+3)}$	$\frac{J(J+2)(6J+5)}{60(2J+1)(2J+3)}$
$[J, J+1, J+1, J+1]$	$\frac{-J}{30}$	$\frac{-J}{60}$
$[J, J+1, J+2, J+1]$	$\frac{-(J+1)(J+3)}{15(2J+3)}$	$\frac{-(J+1)(J+3)}{30(2J+3)}$

four-photon process with a similar sequence of electronic angular momenta of the states involved.

2.2 *Excited state parametric and non-parametric CARS*

In a previous study it was shown that in I_2 different resonance FWM processes $\omega_3 = 2\omega_1 - \omega_2$ occur. In the present work two of these CARS processes are studied as a function of the relative orientations of the linear polarization of the beams. The resonances in both processes, the parametric and non-parametric excited-state CARS, are shown in figure 1. The expressions for the third-order susceptibility in these processes, for a certain line at frequency ω, were derived to be [4]

$$\chi^{(3)}_{\text{par.}\,\rho\sigma\tau\nu}(\omega_3) =$$

$$N \sum_{M_0,M_a,M_b,M_c} \sum_b \rho^{(0)}_{00} \frac{\langle 0|\mu^\sigma|a\rangle\langle a|\mu^\tau|b\rangle\langle b|\mu^\nu|c\rangle\langle c|\mu^\rho|0\rangle}{(\omega_{a0} - \omega_1 - i\Gamma_{a0})(\omega_{b0} - 2\omega_1 - i\Gamma_{b0})(\omega_{c0} - \omega_3 - i\Gamma_{c0})},$$

$$\chi^{(3)}_{\text{non-par.}\,\rho\sigma\tau\nu}(\omega_3) =$$

$$N \sum_{M_0,M_a,M_b,M_c} \sum_b \rho^{(0)}_{00} \frac{\langle 0|\mu^\sigma|a\rangle\langle a|\mu^\tau|b\rangle\langle b|\mu^\rho|c\rangle\langle c|\mu^\nu|0\rangle}{(\omega_{a0} - \omega_1 - i\Gamma_{a0})(\omega_{ac} - \omega_1 + \omega_2 - i\Gamma_{ac})(\omega_{bc} - \omega_3 - i\Gamma_{bc})}$$

$$- N \sum_{M_0,M_a,M_b,M_c} \sum_b \rho^{(0)}_{00} \frac{\langle 0|\mu^\sigma|a\rangle\langle a|\mu^\tau|b\rangle\langle b|\mu^\rho|c\rangle\langle c|\mu^\nu|0\rangle}{(\omega_{c0} - \omega_2 + i\Gamma_{c0})(\omega_{ac} - \omega_1 + \omega_2 - i\Gamma_{ac})(\omega_{bc} - \omega_3 - i\Gamma_{bc})}. \tag{21}$$

The $\chi^{(3)}$ terms contributing to the non-parametric excited-state CARS consist of a pressure induced extra resonance (PIER4) part [18] and a part which is not pressure induced.

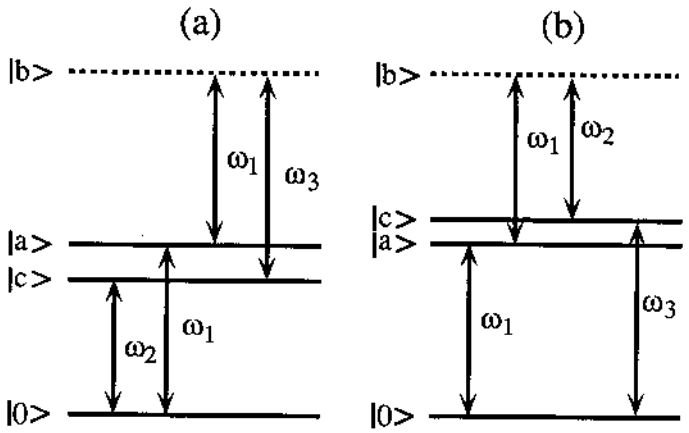

Figure 1. (a) Energy diagram corresponding to non-parametric excited-state CARS. Dashed lines indicate a continuum. (b) Energy diagram corresponding to parametric excited-state CARS.

It is important to notice that the sequence of transition dipole matrix elements is the same for the two terms of the non-parametric CARS process, so that both terms will yield the same rotational linestrength factors. Furthermore, the sequence of matrix elements is different for the parametric and non-parametric resonance CARS process. Different rotational linestrength factors S^{0abc}_{jklm} are, therefore, expected for the two CARS processes.

For the axes defined in section 2.1 (all $\boldsymbol{k}$ vectors along the y axis and ω_1 pump beam polarization along the z axis) it was shown that for arbitrary orientation of the linear polarization of the incoming ω_2 beam only the elements $\chi^{(3)}_{zzzz}$ and $\chi^{(3)}_{xzzx}$ are needed (see (3)–(5)). A correspondence between $\chi^{(3)}_{\rho\sigma\tau\nu}$ tensor elements (in Cartesian coordinates) and rotational linestrength factors S^{0abc}_{jklm} (in spherical components) is established by (19). For a particular FWM process (as in (21)) the order of the components of the dipole operator in the matrix elements needs to be considered. For the parametric process the rotational linestrength factors for the $\chi^{(3)}_{zzzz}$ and $\chi^{(3)}_{xzzx}$ tensor elements are determined by the spherical components S_{0000} and S_{100-1}, respectively. In the case of the non-parametric process, however, the indices ν and ρ are interchanged compared to the parametric process (see (21)). The linestrength factors of the $\chi^{(3)}_{zzzz}$ and $\chi^{(3)}_{xzzx}$ elements of the non-parametric CARS process are, therefore, S_{0000} and S_{1001}, respectively. Using of (20) it can be proven that S_{100-1} and S_{-1001} are identical, and as a result we find that the rotational linestrength factors for parametric and non-parametric resonance CARS are identical.

Also the linestrength factors for the $\chi^{(3)}_{xxzz}$ and $\chi^{(3)}_{xzxz}$ elements were calculated and it was verified that the S factors were consistent with the relation

$$\chi^{(3)}_{zzzz} = \chi^{(3)}_{xzzx} + \chi^{(3)}_{xxzz} + \chi^{(3)}_{xzxz}. \tag{22}$$

This relation is known to hold generally for FWM in isotropic media. In our calculations the isotropy of the medium was introduced by the summation over all M_0 components of the states $|0\rangle$, $|a\rangle$, $|b\rangle$ and $|c\rangle$ in (20).

From the line positions in the FWM spectra the states $|0\rangle$, $|a\rangle$ and $|c\rangle$ in the excited-state parametric and non-parametric CARS processes could be assigned [4]. State $|0\rangle$ belongs to the electronic ground state $X^1\Sigma_g^+$ ($\Omega = 0$), whereas $|a\rangle$ and $|c\rangle$

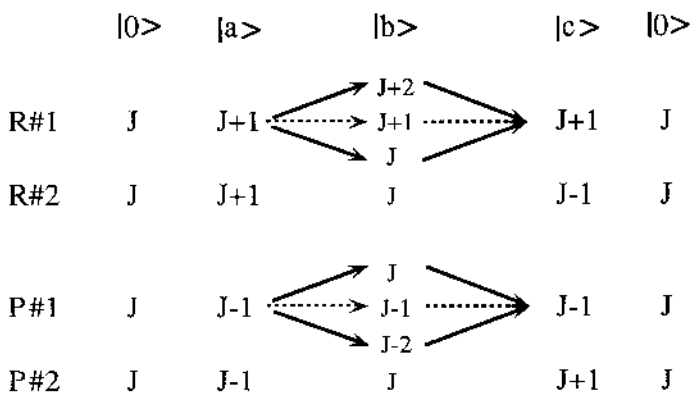

Figure 2. Diagrammatic representation of J-state sequences involved in a $[J_0, J_a, J_b, J_c]$ four-wave mixing cycle. Starting with an R-transition in the first-photon interaction, component #1 in a doublet involves a $(J + 1)$ level in the $|c\rangle$-state. In case of $\Omega_b = 0$ there are only two arrows, and in case of $\Omega_b = 1$ there are three (including the dashed line) routes through the $|b\rangle$-state. For component #2 a $(J - 1)$ level in the $|c\rangle$-state is involved and there is only one possible path for either $\Omega_b = 0$ or 1. Similar for a four-wave mixing cycle with a P-transition in the first one-photon resonance.

both belong to the electronic excited state $B^3\Pi_{u0}^+$ ($\Omega = 0$). The identification of state $|b\rangle$ is somewhat more difficult when only line positions are considered. From selection rules it follows that the $|b\rangle$ state either has $\Omega = 0$ or 1 symmetry. This is the reason that values for the rotational line strengths for both possibilities are given in tables 1 and 2. In the literature evidence is presented [19, 20] that a repulsive state 0_g^+ at the two-photon energy at 37 700 cm^{-1} exists. It was postulated by Aben *et al.* [4] that this 0_g^+-state is probed through the $2\omega_1$- and ω_3-resonance in the parametric and non-parametric process, respectively. The summation over $|b\rangle$ in the expression for $\chi^{(3)}$ is maintained in (21) to take into account the enhancement of all possible FWM cycles through this continuum. Independent of the value of Ω_b the same continuum enhances both CARS processes (see figure 1).

Now we focus on the analytical expressions for the rotational linestrengths. In figure 2 the four-photon cycles contributing to the rotational line strengths of particular FWM resonances are shown graphically. Firstly, cycles starting with P or R resonances can be distinguished. For a certain vibronic state $|c\rangle$, two possible J_c values are allowed by the Clebsch-Gordan coefficients in (20), namely $J_c = J_0 - 1$ and $J_c = J_0 + 1$. It follows that doublets, indicated by routes 1 and 2 in figure 2, can be identified for which $|0\rangle$, $|a\rangle$, $|b\rangle$ and $|c\rangle$ are identical, except for the rotational part of state $|c\rangle$.

The possible J_b states in the continuum which must be considered also follow from the Clebsch-Gordan coefficients. For a given line in the FWM spectrum, so a certain (J_0, J_a, J_c) combination, the possible J_b values depend on the value of Ω_b. In the case of $\Omega_b = 0$ the #1 component of the doublet may be enhanced by the $|b\rangle$ state through two different routes: one with $J_b = J_a + 1$ and one with $J_b = J_a - 1$. For $\Omega_b = 1$ the Clebsch-Gordan coefficients also allow a third route through the $|b\rangle$ state continuum, namely $J_b = J_a$. Within a doublet the components #1 of figure 2 refer to spectral features with contributions of different coinciding cycles, whereas components 2 represent spectral lines involving a single FWM cycle. In tables 3 and 4 the

Table 3. Rotational line strength S for a Hund's case (c), where $\Omega_0 = \Omega_a = \Omega_b = \Omega_c = 0$. Different J routes contributing to one line in the FWM spectrum have been summed.

Component	Routes	Parallel polarization	Crossed polarization
R # 1	$[J, J+1, J+2, J+1] + [J, J+1, J, J+1]$	$\frac{(J+1)(4J+3)}{15(2J+1)}$	$\frac{-(J+1)(J+2)}{30(2J+1)}$
R # 2	$[J, J+1, J, J-1]$	$\frac{2J(J+1)}{15(2J+1)}$	$\frac{-J(J+1)}{10(2J+1)}$
P # 1	$[J, J-1, J-2, J-1] + [J, J-1, J, J-1]$	$\frac{J(4J+1)}{15(2J+1)}$	$\frac{-J(J-1)}{30(2J+1)}$
P # 2	$[J, J-1, J, J+1]$	$\frac{2J(J+1)}{15(2J+1)}$	$\frac{-J(J+1)}{10(2J+1)}$

Table 4. Rotational line strength S for a Hund's case (c), where $\Omega_0 = \Omega_a = \Omega_c = 0$ and $\Omega_b = 1$. Different J routes contributing to one line in the FWM spectrum have been summed.

Component	Routes	Parallel polarization	Crossed polarization
R # 1	$[J, J+1, J+2, J+1] + [J, J+1, J, J+1]$ $+ [J, J+1, J+1, J+1]$	$\frac{-(J+1)(3J+1)}{15(2J+1)}$	$\frac{-(J+1)(J+2)}{60(2J+1)}$
R # 2	$[J, J+1, J, J-1]$	$\frac{J(J+1)}{15(2J+1)}$	$\frac{-J(J+1)}{20(2J+1)}$
P # 1	$[J, J-1, J-2, J-1] + [J, J-1, J, J-1]$ $+ [J, J-1, J-1, J-1]$	$\frac{-J(3J+2)}{15(2J+1)}$	$\frac{-J(J-1)}{60(2J+1)}$
P # 2	$[J, J-1, J, J+1]$	$\frac{J(J+1)}{15(2J+1)}$	$\frac{-J(J+1)}{20(2J+1)}$

Table 5. Ratio of rotational line strength factors $S_{J_c=J+1}/S_{J_c=J-1}$ for a Hund's case (c) with $\Omega_0 = \Omega_a = \Omega_c = 0$.

		Parallel	Crossed
$J_a = J + 1$:	$\Omega_b = 0$	$\frac{4J + 3}{2J}$	$\frac{J + 2}{3J}$
	$\Omega_b = 1$	$\frac{-(3J + 1)}{J}$	$\frac{J + 2}{3J}$
$J_a = J - 1$:	$\Omega_b = 0$	$\frac{2(J + 1)}{4J + 1)}$	$\frac{3(J + 1)}{J - 1}$
	$\Omega_b = 1$	$\frac{-(J + 1)}{3J + 2}$	$\frac{3(J + 1)}{J - 1}$

rotational line strengths, with contributions of all routes contributing to the same line added, are given for both lines in the doublet.

The 'resonance factors' in the denominator of (21) are assumed to be identical for different J_c (and J_b) values. This is the case when the damping parameters Γ_{b0} and Γ_{c0} are independent of J. By taking the ratio of two corresponding components in a doublet the 'resonance factors' cancel and the relative intensities are determined only by the corresponding differences in rotational line strength. This procedure has the additional advantage that effects of the relative population $N\rho_{00}^{(0)}$ of the ground states probed also drop out. The ratios of line strengths are tabulated in table 5 for different polarizations and different Ω_b. The values are given for the lines in doublets corresponding to $J_a = J_0 + 1$ and $J_a = J_0 - 1$. From these tables relative intensities within a doublet in a FWM spectrum for parallel as well as crossed polarizations, can easily be obtained by squaring the appropriate values. In the case of polarizations at an angle α (5) must be used. Here the intensity is given in terms of a geometrical weighing factor of the two extreme cases of parallel and crossed polarization.

3. Experiments on line intensities in CARS; comparison with theory

The set-up for the experimental part of this study was described in detail in a previous paper [4]. The output of an injection-seeded frequency doubled Nd–YAG laser at $\omega_1 = 18\,788{\cdot}3(2)\,\mathrm{cm}^{-1}$ with a bandwidth of $0{\cdot}005\,\mathrm{cm}^{-1}$ was used in part to pump a pulsed dye laser (ω_2) operating on different rhodamine dyes. In the previous study a Quanta Ray PDL-2 dye laser with a bandwidth of $0{\cdot}3\,\mathrm{cm}^{-1}$ was used while in the present study a PDL-3 dye laser with a bandwidth of $0{\cdot}07\,\mathrm{cm}^{-1}$ was employed. The beams at frequencies ω_1 and ω_2 were overlapped collinearly with a dichroic mirror. CARS signals at $\omega_3 = 2\omega_1 - \omega_2$ were generated in a focused geometry with f = 25 cm lens. Using a bandpass filter and a three-stage monochromator, the ω_3 wave was separated from the fundamental frequencies and detected on a photomultiplier.

The polarization of the beam at $\lambda_1 = 532\,\mathrm{nm}$ was rotated using a $\lambda/2$ plate. The value of the relative polarization angle could be determined with an accuracy of $\pm 2°$. As the reflection coefficient of the dichroic mirror varies with the degree of polarization rotation of the ω_1 beam, absolute intensities in spectra taken at different relative polarizations could not be compared. In the present study we focused on relative

intensities between components of doublets, recorded in single scans at fixed relative polarization orientations.

3.1. *Non-parametric excited state CARS*

In figure 3 spectra are shown for the non-parametric excited state CARS process recorded for frequency combinations (ω_1, ω_2) with ω_1 fixed at 18 788·3 cm^{-1} and ω_2 tuned over the energy range 17 475–17 488 cm^{-1}. The Raman shift ($\omega_1 - \omega_2$) is around 1305 cm^{-1} as denoted in the figure. The upper spectrum was recorded for nearly parallel polarization ($\alpha = 3°$), whereas, in the lower part crossed polarizations ($\alpha = 91°$) were used. The middle one was taken at $\alpha = 69°$.

We recall here from Aben *et al.* [4] that the fixed frequency ω_1 selects certain states $|0\rangle$ and $|a\rangle$ for which ω_1 is in (near) resonance. Mainly the FWM processes involving the resonances $X^1\Sigma_g^+$, $v_0 = 0$, $J_0 = 53 \rightarrow B^3\Pi_{u0}^+$, $v_a = 32$, $J_a = 52$, and $X^1\Sigma_g^+$, $v_0 = 0$, $J_0 = 56 \rightarrow B^3\Pi_{u0}^+$, $v_a = 32$, $J_a = 57$ are enhanced through the fixed ω_1 frequency at 18 788·3(2) cm^{-1}. They are referred to as P(53) and R(56) respectively throughout the rest of the paper. Tuning ω_2 yields the FWM spectrum. The features of figure 3 are also resonantly enhanced by the $B^3\Pi_{u0}^+$, $v_c = 16$ intermediate state in I_2 (representing state $|c\rangle$ of figure 1 (a)).

In the spectra several resonance doublets could be identified that probe a common ground state population. The members of such a doublet could easily be related on the basis of the positions in the spectrum (see [4]) and are marked as such in figure 3. They only differ in the value of J_c. One (P(53)) corresponds to ($J_0 = 53$, $J_a = 52$) with $J_c = 54$ and 52, while another (R(56)) belongs to ($J_0 = 56$, $J_a = 57$) with $J_c = 57$ and 55. A third doublet of FWM resonances is related to the coincidental enhancement by the $B^3\Pi_{u0}^+$, $v_c = 17$ P(103) resonance. One of the lines of that doublet, which will not be considered further, appears in the range of the spectrum of figure 3. As an indication for the relative intensities in the doublets the expressions in table 5 can be used in the high J limit. In the case of parallel polarization intensity ratios $|S_{J_c=J+1}/S_{J_c=J-1}|$ of 4 : 1 are expected when $\Omega_b = 0$, and 9 : 1 if $\Omega_b = 1$ for both doublets. The stronger lines in the doublets are ($J_0 = 53$, $J_a = 52$, $J_c = 52$) and ($J_0 = 56$, $J_a = 57$, $J_c = 57$). In the case of crossed polarizations in both cases ($\Omega_b = 0$ or $\Omega_b = 1$) an intensity ratio of 1 : 9 is predicted.

These trends are reflected in the observed spectra of figure 3. For example, in the doublet ($J_0 = 56$, $J_a = 57$) at parallel polarizations the component with $J_c = J_0 + 1$ is about four times stronger than the component with $J_c = J_0 - 1$. This ratio turns around in favour of the $J_c = J_0 - 1$ component when going from $\alpha = 0°$ to 90°.

The intensity ratios within the doublets were measured and also calculated for a wide variety of relative polarization angles. Experimental intensities were determined by integrating the signal over the widths of the different peaks involved. The calculation of the ratios of line intensities for arbitrary polarization was performed by using the closed-form expressions in tables 3 and 4 for $J_0 = 53$ or 56 in combination with (5). In figure 4 (a) the ratio of observed intensities for components of the doublet P(53) are plotted as a function of angle α. The intensity ratios between two components are displayed on a log-scale so as to visualize deviations from theory at $\alpha = 0°$ (#1/#2 large) and $\alpha = 90°$ (#2/#1 large) with an equal emphasis. Theoretical curves based on the assumptions $\Omega_b = 0$ and $\Omega_b = 1$ are plotted as well. In figure 4(b) ratios of observed and calculated intensities for the doublet R(56) are shown. For both P(53) and R(56) doublets there is good agreement between the observed intensity ratios and

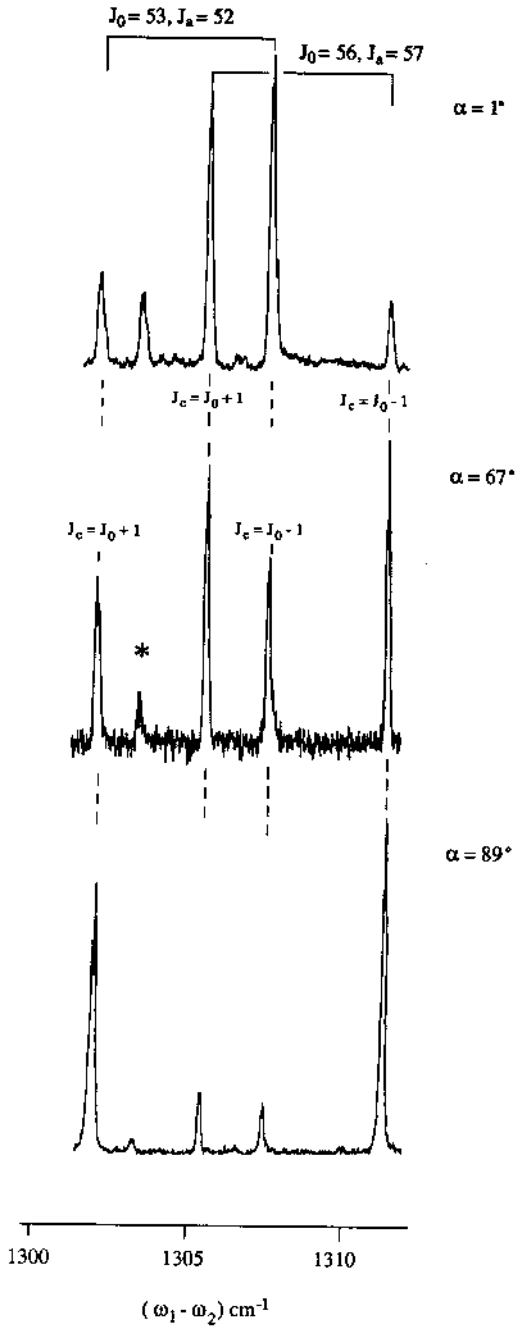

Figure 3. Observed four-wave-mixing spectrum in I_2 (non-parametric excited-state CARS) for three different orientations of the relative polarization of the two incoming beams. α denotes the angle between polarization vectors.

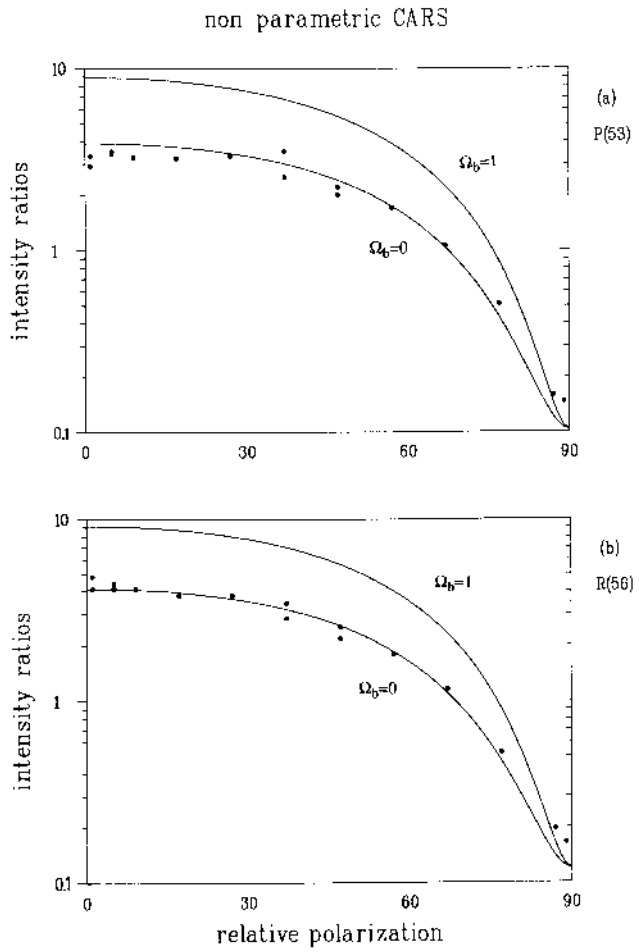

Figure 4. Calculated curves (for both $\Omega_b = 0$ and 1) and observed intensity ratios as a function of the relative polarization for the non-parametric excited-state CARS. The intensity ratios are given on a log-scale. (a) Doublet for P(53) resonance as defined in the text in section 3.1; (b) same for R(56).

the theoretical prediction based on an intermediate state with $\Omega_b = 0$. Enhancement by a continuum state $|b\rangle$ with $\Omega_b = 1$ can be definitely excluded.

In summary, agreement between theory and experiment is excellent for all angles α except for α close to 90° where some deviations occur. Here it has to be noticed that experimental conditions of pure polarization are difficult to realize. Some elliptical polarization components are always present. Hence, the conditions of perpendicular or parallel polarizations are never met. The theoretical curves show that the intensity ratios near crossed polarizations strongly change with the angle α. Elliptical polarization components, therefore, affect the intensity ratios predominantly in the regime of near crossed polarizations.

3.2. *Parametric excited-state CARS*

In figure 5 recorded spectra are shown for the parametric excited-state CARS for

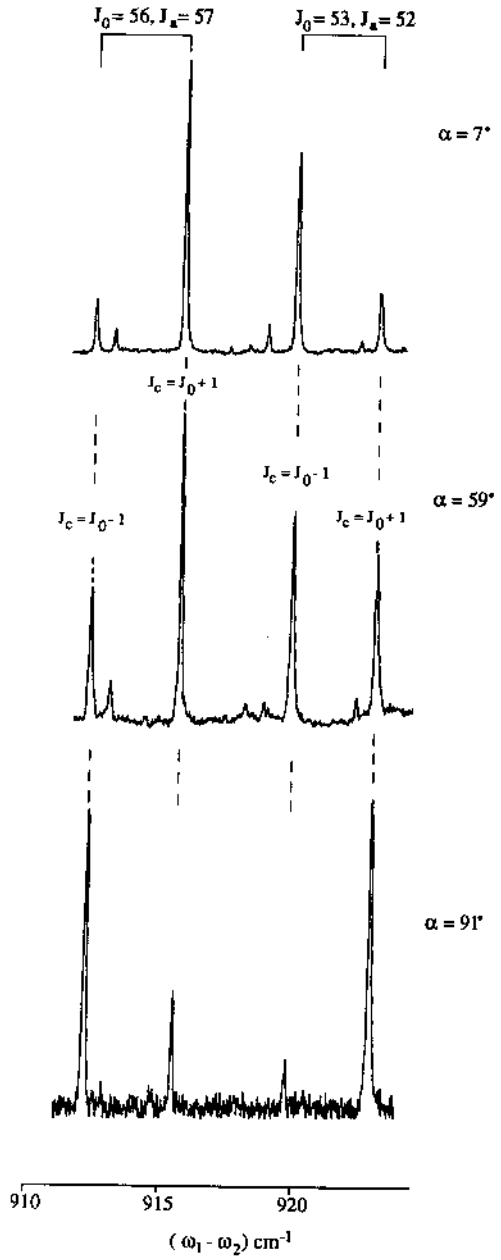

Figure 5. Observed four-wave-mixing spectrum in I_2 (parametric excited-state CARS) for three different orientations of the relative polarization of the two incoming beams. α denotes the angle between polarization vectors.

Raman shifts ($\omega_1 - \omega_2$) in the range between 910 and 925 cm^{-1}, with ω_1 again fixed at 18 788·3 cm^{-1}. The upper spectrum corresponds to nearly parallel polarization ($\alpha = 7°$), the lower to crossed polarizations ($\alpha = 91°$), and the middle to $\alpha = 59°$.

The FWM features in this case originate from discrete state resonance enhancement on $B^3\Pi_{u0}^+$ $v = 32$, $J = 52$ and 57 levels in I_2 probed by ω_1 and $B^3\Pi_{u0}^+$ $v = 53$,

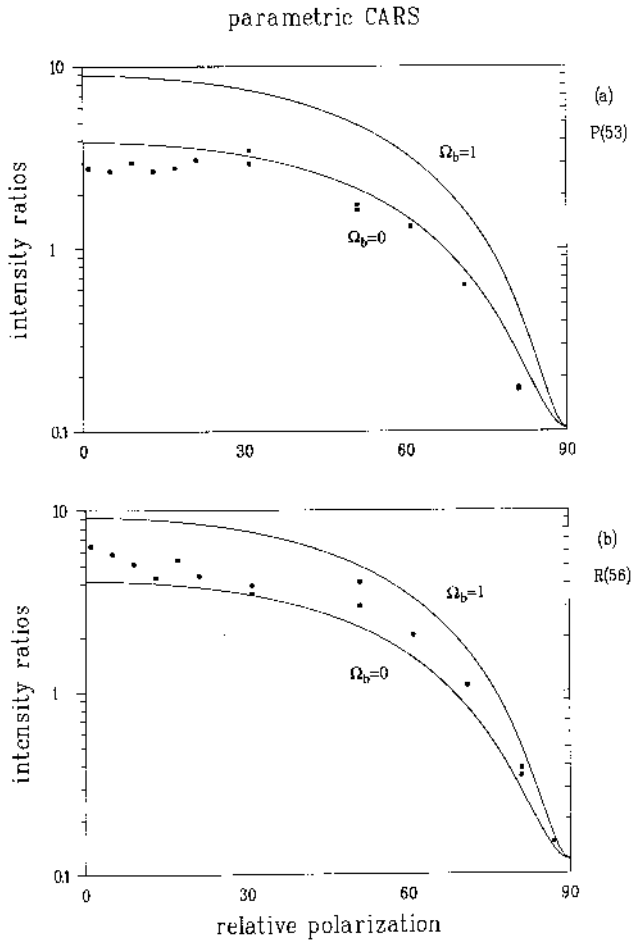

Figure 6. Calculated curves (for both $\Omega_b = 0$ and 1) and observed intensity ratios as a function of the relative polarization for the parametric excited state CARS. The intensity ratios are given on a log-scale. (a) Doublet for P(53) resonance as defined in the text in section 3.2; (b) same for R(56).

J_c at an energy of $2\omega_1 - \omega_2$ [4]. Similar to the case of non-parametric excited state CARS the two doublets in the spectra correspond to ($J_0 = 53$, $J_a = 52$) and ($J_0 = 56$, $J_a = 57$). The members of these doublets are indicated in figure 5.

As mentioned in section 2.2 the predictions concerning the intensity ratios for the components of a doublet in a parametric excited-state CARS process are identical to the values in the non-parametric process. Indeed we find again, e.g. on the ($J_0 = 56$, $J_a = 57$) doublet in figure 5, that the intensity ratio of the $J_c = J_0 + 1$ and $J_c = J_0 - 1$ components changes drastically in going from parallel to crossed polarizations.

The intensity ratios within these doublets were again measured for a wide variety of relative polarization angles. The results are plotted in figures 6(a) and 6(b) for P(53) and R(56) doublets, respectively. Note that the theoretical curves are identical to those of figure 4. Although the observed intensity ratios (with angular variation) of the relative polarization orientation follows the trend of the calculated values, the detailed agreement is not as satisfactory here as in the case of the non-parametric

process (section 3.1). Disregarding the significant spread in the intensity ratio, reflecting the lower signal-to-noise for the parametric CARS resonances, a systematic discrepancy shows between observed and calculated values. At $\alpha = 0°$ the intensity ratios in the P(53) and R(56) doublets are 3 : 1 and 5 : 1, respectively, where the ratio of 4 : 1 is expected assuming a $\Omega_b = 0$ continuum state.

In a previous paper [4] we already remarked that resonances of the 'laser-enhanced CARS process' introduced by Attal *et al.* [3] coincide with the resonances of the parametric FWM scheme of figure 1 (b). In their laser-enhanced CARS process the continuum resonance at the $2\omega_1$ level is replaced by resonance enhancement (with a detuning $\delta\omega_i$) on rovibrational levels of the $\Omega = 0$ ground state of I_2. Also, these detunings are different for sequences starting with P(53) or R(56). Contribution from this alternative scheme might explain the discrepancy between theory and experiment in this case.

4. Concluding remarks

In the present investigation it was shown that observed intensity ratios as a function of polarization for different rotational line components in excited-state CARS agree reasonably well with calculations of line strengths in four-photon coherent processes. Agreement for the non-parametric process was considerably better than for the parametric process. Although in the latter FWM process signal intensities and therewith signal-to-noise ratios are lower and the scatter in the results larger (compare figure 6 for the parametric process with e.g. figure 4 for the non-parametric process) this cannot explain the deviations from the theoretical intensity ratios. A systematic difference between relative line strengths between components in doublets related to P(53) and R(56) transitions in this parametric FWM process is apparent and might be attributed to the effect of other processes such as the 'laser enhanced CARS processes'. The intensity ratios of the P(53) doublet are lower while the ratios for the R(56) doublet are higher than the theoretical value for all angles of relative polarization of the incoming beams.

A few comments on the general applicability of the rotational line strengths derived for coherent four-photon processes in tables 1 to 5 can be made. Firstly, these line strength relations were derived in view of the experiments in I_2, so an electronic angular momentum Ω was defined referring to a Hund's coupling case (c). The relations are straightforwardly applicable for Hund's case (a) single states, when Ω is replaced by an electronic orbital angular momentum Λ. Secondly, the rotational line strength expressions were derived for a collinear $\boldsymbol{k}$-vector geometry of incoming waves. In other wave-mixing geometries such as BOXCARS the effect of incident angles between wave vectors has to be accounted for.

Finally we note that the expressions for rotational line strengths of table 1 are applicable to degenerate four-wave-mixing processes in molecular gases with a $^1\Sigma$ ground and $^1\Sigma$ excited state. The expression for $[J, J-1, J, J-1]$ holds for a P transition while $[J, J+1, J, J+1]$ relates to an R transition, also it is not necessary that the transition moments in (9)–(15) have an electronic origin. Replacing of $\boldsymbol{\mu}$ by a permanent dipole moment and interpreting the photon interactions in terms of vibrational transitions in molecules leave the expressions unchanged. As such two of the expressions of table 1 are relevant for the description of rotational line strengths for DFWM processes in HF [21].

References

[1] Ewart, P., and O'Leary, S. V., 1986, *Opt. Lett.*, **11,** 279.
[2] Dreier, T., and Rakestraw, D. J., 1990, *Appl. Phys.*, **B50,** 479.
[3] Attal, B., Schnepp, O. O., and Taran, J.-P., 1978, *Optics Commun.*, **24,** 77.
[4] Aben, I., Ubachs, W., Levelt, P., vd Zwan, G., and Hogervorst, W., 1991, *Phys. Rev.*, **A44,** 5881.
[5] Attal-Trétout, B., and Bouchardy, P., 1987, *La Rech. Aerosp.*, **5,** 19.
[6] Amal, B., Debarre, D., Müller-Dethlefs, K., and Taran, Y. P. E., 1983, *Rev. Phys. Appl.*, **18,** 39.
[7] McIllwain, H. E., and Hindman, J. C., 1980, *J. Chem. Phys.*, **73,** 68.
[8] Guthals, D. M., Gross, K. P., and Nibler, J. W., 1979, *J. Chem. Phys.*, **70,** 2393.
[9] Beckman, A., Fietz, H., Baierl, P., and Kiefer, W., 1982, *Chem. Phys. Lett.*, **86,** 140.
[10] Mainos, C., Le Duff, Y., and Boursey, E., 1985, *Molec. Phys.*, **56,** 1165.
[11] Aguillon, F., Lebehot, A., Rousseau, J., and Campargue, R., 1987, *J. Chem. Phys.*, **86,** 5246.
[12] Merkt, F., and Softley, T. P., 1991, *Molec. Phys.*, **72,** 787.
[13] Attal-Trétout, B., Monot, P., and Müller-Dethlefs, K., 1991, *Molec. Phys.*, **73,** 1257.
[14] Luc, P., 1980, *J. Molec. Spectrosc.*, **80,** 41.
[15] Shen, Y. R., 1984, *The Principles of Nonlinear Optics* (Wiley).
[16] Prior, Y., 1984, *I.E.E.E. J. quant. Electron.*, **QE20,** 37.
[17] Zare, R. N., 1988, *Angular Momentum* (Wiley).
[18] Prior, Y., Bogdan, A. R., Dagenais, M., and Bloembergen, N., 1981, *Phys. Rev. Lett.*, **46,** 111.
[19] Sander, R. K., and Wilson, K. R., 1975, *J. Chem. Phys.*, **63,** 4242.
[20] Kasatani, K., Tanaka, Y., Shibuga, K., Kawasuki, M., Obi, K., Sato, H., and Tanaka, I., 1981, *J. Chem. Phys.*, **74,** 895.
[21] Van der Wal, R. L., Holmes, B. E., Farrow, R. L., Jeffries, J. B., and Rakestraw, D. J., CLEO 1991 Technical Digest Series OSA Vol. 10, p. 384.